

Article

Performance Analysis of an Ammonia-Fueled Micro Gas Turbine

Vittorio Bonasio and Silvia Ravelli * 

Department of Engineering and Applied Sciences, University of Bergamo, Viale Marconi 5, 24044 Dalmine, Italy; v.bonasio@studenti.unibg.it

* Correspondence: silvia.ravelli@unibg.it; Tel.: +39-035-2052346

Abstract: Micro gas turbines fit perfectly with the energy roadmap to 2050: on-site, small scale power generation, combined with heat recovery from exhaust gas, offers an opportunity to deploy primary energy saving and pollutant emission reduction. Moreover, their flexibility enables fuel switching from natural gas (NG) to carbon-free fuels such as hydrogen and ammonia. This study aims to explore the potential of direct combustion of ammonia in a micro gas turbine (MGT), from a thermodynamic point of view. A modeling procedure was developed to simulate the behavior of a 100 kW MGT operating at full and part-load. After validation with NG as fuel, an increasing fraction of ammonia was fed to the combustor to predict performance variations in terms of electric, thermal and total efficiency, as well as exhaust gas composition, for a load range between 40% and 100%. Additional relevant details, related to the interaction between compressor and turbine in the single-shaft arrangement, were discussed through performance maps. Full replacement of NG with ammonia was found to reduce electric efficiency by about 0.5 percentage points (pp), whatever the power output, with a consequent improvement in exhaust gas heat recovery. Thus, total efficiency is maintained at a high level, with values ranging from 74.5% to 79.1% over the investigated load range. The benefit of zero CO₂ emissions can be achieved provided that compressor–turbine matching is adjusted to compensate for the reduction in fuel calorific value: at rated power, when the largest fuel input is required, flow rates of air and flue gas decrease by 4.3% and 2.8%, respectively, with an increase in Brayton cycle pressure ratio of 2%.

Keywords: micro gas turbine; off-design; part-load; fuel flexibility; ammonia; decarbonization



Citation: Bonasio, V.; Ravelli, S. Performance Analysis of an Ammonia-Fueled Micro Gas Turbine. *Energies* **2022**, *15*, 3874. <https://doi.org/10.3390/en15113874>

Academic Editor: Artur Blaszczyk

Received: 5 May 2022

Accepted: 22 May 2022

Published: 24 May 2022

Publisher's Note: MDPI stays neutral with regard to jurisdictional claims in published maps and institutional affiliations.



Copyright: © 2022 by the authors. Licensee MDPI, Basel, Switzerland. This article is an open access article distributed under the terms and conditions of the Creative Commons Attribution (CC BY) license (<https://creativecommons.org/licenses/by/4.0/>).

1. Introduction

The global demand for carbon-free power generation is pushing the boundaries of research into alternative fuels deriving from renewable sources: they can be produced from electricity when supply capacity exceeds demand. The so called “e-fuels” such as e-hydrogen, e-ammonia, e-methane, e-methanol, or e-diesel are actually opening up a new path to the future. The former can be used straightaway in a prime mover, but its widespread application as a practical fuel still faces several shortcomings in several respects [1]. Starting from the production phase, lower renewable costs are not enough to make green hydrogen cost competitive by 2030: electrolysis needs to be scaled up from MW to GW levels through continuous innovation and performance improvements [2]. For storage, challenges are mainly the weight, volume, cost, efficiency, as well as codes and standards. Due to the low volumetric energy density, hydrogen utilization suffers from high cost of back production in the case of compressed gas or liquid stream and low storage capacity in the case of solid carriers [3]. When dealing with delivery and distribution, the main issue is that a new infrastructure would be required as a function of the technology chosen for large-scale hydrogen storage [4]. Unfortunately, there is no ideal solution for all stationary and automotive applications but a set of complementary production and delivery systems that must be integrated to reduce the overall hydrogen cost [5]. Indeed,

advantages of e-fuels other than hydrogen include higher energy density so that they can be transported conveniently over long distances and kept in large scale stationary storage to compensate seasonal supply fluctuations. Moreover, existing infrastructure can continue to be used [6].

Among all the options available, green hydrogen can be stored in the form of ammonia, as ammonia offers higher volumetric energy density and thus greater convenience of storage and transport, as well as excellent safety and long-term stability. In particular, liquid ammonia is of interest, especially at mild conditions: being similar to propane, much of the necessary infrastructure required for handling and transport is already in place, with well-established regulations for operations and storage [7].

On the one hand, ammonia can be cracked back into hydrogen (and nitrogen) on demand [8], thus serving as a hydrogen carrier.

On the other hand, ammonia is receiving unprecedented attention as a zero-carbon fuel for direct power generation [9]. Direct feeding to a solid oxide fuel cell has been reported to show a comparable performance to that with hydrogen even though commercial availability to the market has yet to be reached [10]. Alternatively, combustion based technologies rely on internal combustion engines and gas turbines, being aware that thermal properties and combustion characteristics of ammonia require innovation [11].

In the former case, a dual-fuel approach is recommended with the other fuel (gasoline or diesel) acting as combustion promoter, due to ammonia's low flame speed and high resistance to auto-ignition [12]. More specifically, in spark-ignition engines, ammonia can be blended with hydrogen, gasoline, NG, etc., while in compression-ignition engines it can be blended with diesel and dimethyl ether (DME) [13]. In the latter case, ammonia has been considered an economically viable option for micro gas turbines used for distributed power generation, as it allows for zero carbon emissions without the unaffordable cost and complexity of CO₂ sequestration [14].

NH₃-air power generation using a 50 kW class MGT was stably operated by Kurata et al. [15], over a wide range of power and rotational speeds, i.e., 18.4–44.4 kW and 70,000–80,000 rpm, respectively. The combustion efficiency ranged from 89% to 96% at the highest rotational speed. A regenerative cycle was adopted to take advantage of combustor inlet temperature higher than 500 °C, thus lowering unburnt NH₃. Gaseous NH₃ and diffusion combustor contributed to the flame stabilization [16]. Flame observations made it clear that emissions of NO and NH₃ depend on combustor inlet temperature [17]. Indeed, the greatest efforts focused on experimental investigation of NO_x reduction strategies, by varying the fuel mixture. For a premixed swirling NH₃/H₂ flame, NO_x levels strongly depend on the operational equivalence ratio [18]. When comparing swirl stabilized premixed vs. diffusion NH₃-air flame, the latter delivered substantially lower NO concentrations at leaner conditions [19]. In a highly humidified 70%NH₃-30%H₂ blend, a stable flame was obtained even under highly humidified conditions but, more important, NO_x emissions decrease with the increase in the injected steam [20]. In a small-scale Siemens burner used in the SGT-750 gas turbine (GT), flame stability and emissions were characterized as a function of fuel mixtures, with the aim of finding the optimal NH₃-H₂-N₂ fuel blend [21]: the emissions become very low when full decomposition is achieved (H₂/N₂-75/25). Moreover, blended-fuel combustion is aimed at improving flame propagation characteristics: extensive experimental campaigns demonstrated that low reactivity and low-flame-speed issues of pure NH₃/air combustion can be tackled by mixing NH₃ with H₂ [22], CH₄ [23], syngas [24], and DME [25]. As regards combustion strategies in gas turbines, partially premixed combustion has attracted considerable attention recently: it combines the advantages of both premixed and non-premixed combustion so that the equivalence ratio can be extended to about 0.4 while retaining reasonable flame stability and low NO emissions [26].

Research activity has also been active in the field of thermodynamic modeling of gas turbines in a wide range of sizes. An ammonia-fueled combined-cycle gas turbine, including exhaust gas recirculation, was simulated by Keller et al. [27]: GT is operated under fuel-rich conditions and the unburned hydrogen from the GT is burned in the heat-

recovery steam generator. The goal is to maximize the electric efficiency of the system, while maintaining low NO concentration. With the same aim, an improved Brayton cycle fed by humidified ammonia/hydrogen was conceived theoretically by Božo and Valera-Medina [28], through a sensitivity analysis on Brayton cycle pressure ratio and compressor/turbine polytropic efficiency. The maximum cycle efficiency is up to 43.4%; hence, comparable to that of fossil-based systems. At a small scale, the effect of NH_3/CH_4 mixture on exergetic performance of a Turbec T100 MGT was assessed by Ayaz et al. [29]. Three values of ammonia fraction were considered, i.e., 0–10–20%, with the latter being characterized by the lowest environmental impact.

None of the cited modeling studies ([27–29]) accounted for part-load behavior of an ammonia-fueled MGT, which is instead particularly relevant for a prime mover in combined-heat and power (CHP) mode. More generally, the lack of tools predicting the off-design characteristics of an MGT—when integrated with on-site renewable technologies such as solar photovoltaics, wind turbines, as well as battery energy storage, to meet the power demand—was pointed out by Hampel and Braun [30]. They addressed this deficiency by developing a thermodynamic model of a commercial 200 kW MGT to predict part-load control, change in intake air conditions, or change in hot water temperature setpoints for CHP applications, under the assumption of NG/air combustion.

Therefore, there is a need to evaluate MGT performance when an alternative, carbon-free fuel such as ammonia is used, under the impulse of clean energy transition. The relevance of the subject is confirmed by the fact that Horizon2020 EU's research and innovation program financed the project "FLEXnCONFU" in 2020. It is based on Power-to-X-to-Power solutions, in which surplus power from renewable energies is converted into NH_3 prior to converting it back to power. Combustion tests with up to 100% NH_3 are planned in a heavy-duty representative GT combustion system. Moreover, re-design of a micro gas turbine is expected to enable operation with 100% NH_3 for small-scale applications.

This work is intended to provide considerations for the required fuel switching, at part load. Performance maps of rotating components were taken into account to improve the accuracy in off-design conditions: this is important to mimic the actual behavior of the MGT, as highlighted in [31]. The steady-state MGT model is presented in detail, including benchmarking and validation against experimental data: part-load information and assessment of ambient sensitivity are available in the case of NG as fuel. Model validity was also proven with respect to fuel flexibility by examining a single operating point with syngas feeding. The model was then exercised to predict the effects of partial and full replacement of NG with ammonia: variations in electric, thermal, and thus total efficiency were explored in response to reduction in electric load, down to 40%.

2. Assumptions and Method

In the following, a general overview of the modeling procedure is provided including design and off-design conditions. The Turbec T100 Power and Heat unit was chosen as a case study for the availability of technical information [32]. MGT thermodynamic performance was calculated with the help of Thermoflex[®] (Version 29, Thermoflow Inc., Jacksonville, FL, USA). The model incorporates steady-state heat and mass balances: they were solved for each component resulting in an algebraic system of equations with input and output parameters such as pressure, temperature, enthalpy, and mass flow rate. Their convergence tolerance was within 5×10^{-5} , whereas power convergence was within 0.1%, for 4 consecutive loops having up to 60 iterations in each loop.

2.1. Design Modeling

A schematic diagram of the MGT system is shown in Figure 1. The core of the Turbec T100 consists of the components necessary for the regenerative Brayton cycle. The compressor and turbine are mounted on the same shaft as the high-speed generator to produce electricity. An exhaust gas recuperator is included to reduce the fuel consumption. The reference fuel is NG, with a lower heating value (LHV) of 49.56 MJ/kg, fed into a

lean-premixed combustor. The power module is combined with a heat exchanger for CHP applications. At the design point, 100 kW of electric power (P_{el}) are produced with an efficiency of $\eta_{el} = 30\%$ at ISO conditions, with the nominal rotational speed being set at 70,000 rpm.

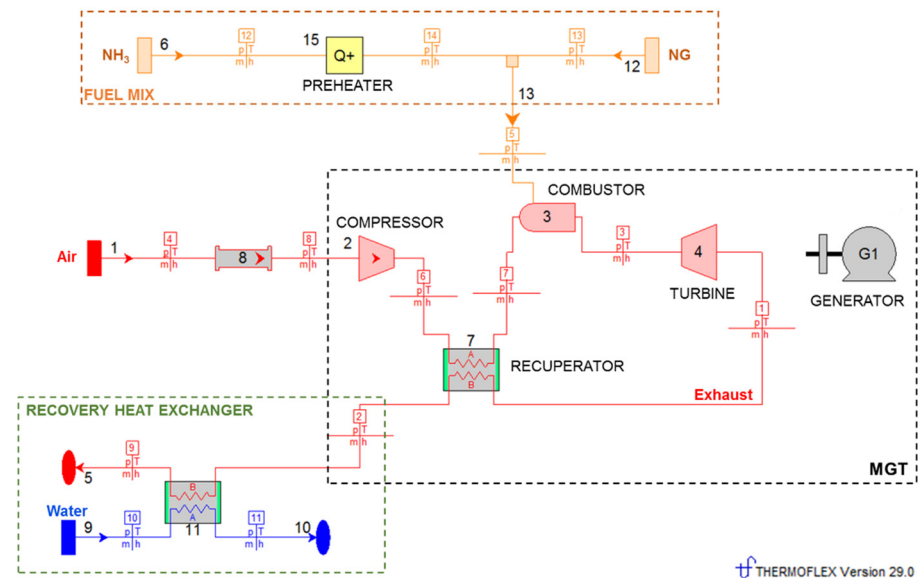


Figure 1. Layout of the micro gas turbine system.

Both compressor and turbine are single-stage, radial turbomachineries with a nominal pressure ratio of β_c and β_{exp} , respectively, equal to about 4.5 bar. Compressed air enters the recuperator to receive the heat energy from the hot exhaust gas flow ($m_{exh} = 0.8$ kg/s). The hot, compressed air mixes with NG to reach a turbine inlet temperature (TIT) of approximately 950 °C. Flue gas leaving the turbine at 650 °C is passed through the recuperator where its temperature drops to 270 °C. In CHP mode, further cooling of the exhaust takes place in the recovery heat exchanger (RHE) to produce hot water: a nominal water flow of 2 l/s is heated up, from the return temperature of 50 °C to the supply temperature of 70 °C. Thermal power (P_{th}) in CHP mode equals 165 kW.

Starting from the information made available by the manufacturer, inputs for setting the design model were established. A key role was played by performance maps of compressor and turbine, taken from published literature [33] and included in Figure A1 in order to allow easier consultation. Given P_{el} , η_{el} , and m_{exh} , simple math operations were required to obtain the fuel flow rate (m_{fuel}) and the airflow (m_a). The latter was essential to characterize the compressor behavior through corrected flow (CF), together with corrected speed (CS). The design point was then identified on the compressor performance map, given β_c . Polytropic efficiency ($\eta_{y,c}$) was deduced from the map whereas isentropic efficiency ($\eta_{is,c}$) was computed through:

$$\eta_{is,c} = \frac{\beta_c^{\frac{\gamma_a - 1}{\gamma_a}} - 1}{\beta_c^{\frac{\gamma_a - 1}{\gamma_a \eta_{y,c}}} - 1} \quad (1)$$

Turning to the turbine, lack of clear indications on its inlet pressure ($p_{in,t}$) made it necessary to iteratively reduce β_{exp} , from the initial estimate of 4.5, until convergence is reached between $p_{in,t}$, turbine outlet pressure ($p_{out,t}$), and pressure drop across combustor, recuperator, and RHE. The resulting values of normalized pressure loss ($\Delta p/p$) are defined as:

$$\frac{\Delta p}{p} = \frac{p_{in} - p_{out}}{p_{in}} \quad (2)$$

where p_{in} and p_{out} are pressure values before and after the loss, listed in Table 1. The turbine design operating point was then found on the turbine performance map, at the intersection of β_{exp} , CS, and corrected flow—defined as inlet flow function (FF)—given m_{exh} , TIT, and $p_{in,t}$. Finally, polytropic efficiency ($\eta_{y,t}$) was estimated from the map, hence obtaining isentropic efficiency ($\eta_{is,t}$) as follows:

$$\eta_{is,t} = \frac{1 - \left(\frac{1}{\beta_{exp}}\right)^{\frac{\gamma_{exh}-1}{\gamma_{exh}}\eta_{y,t}}}{1 - \left(\frac{1}{\beta_{exp}}\right)^{\frac{\gamma_{exh}-1}{\gamma_{exh}}}} \quad (3)$$

Table 1. Normalized pressure loss at the design point.

Component	$\Delta p/p$
Combustor	0.08
Recuperator–air side	0.03
Recuperator–exhaust side	0.05
RHE–exhaust side	0.05
RHE–water side	1

Table 2 summarizes design point features for both the compressor and turbine.

Table 2. Design features of the compressor and turbine.

Compressor			Turbine		
Inlet temperature	K	288.15	Inlet temperature	K	1223.15
Inlet pressure	bar	1.01	Inlet pressure	bar	4.15
Outlet pressure	bar	4.56	Outlet pressure	bar	1.014
Airflow	kg/s	0.7934	Exhaust flow	kg/s	0.8
Corrected flow (CF)	kg-mol/s	0.0276	Corrected flow (FF)	m ²	0.0017
Corrected speed (CS)	rpm	70,000	Corrected speed (CS)	rpm	33,975
Pressure ratio (β_c)		4.5	Pressure ratio (β_c)		4.09
Isentropic efficiency ($\eta_{is,c}$)	%	78.5	Isentropic efficiency ($\eta_{is,t}$)	%	82.9
Polytropic efficiency ($\eta_{y,c}$)	%	82.5	Polytropic efficiency ($\eta_{y,t}$)	%	80.3

As regards the recuperator, the heat transfer from the hot side can be easily obtained from the available information on exhaust flow. Its effectiveness, equal to 89%, is consistent with NG consumption. Complete combustion was assumed: production of carbon monoxide and NOx emissions is disregarded in the analysis. However, the exhaust oxygen level of 17.8% (mol%) is in line with MGT technology, which uses a large amount of excess air [34]. Finally, 9% loss was considered when converting mechanical shaft power into net electric power. The heat recovery section was easily modeled since complete information was provided by the manufacturer, on both cold and hot sides: a normalized heat loss of 1% was set for the RHE to match inlet and outlet temperature on the exhaust side.

MGT performance was evaluated in terms of electric efficiency (η_{el}), thermal efficiency (η_{th}), and total efficiency (η_{tot}):

$$\eta_{el} = \frac{P_{el}}{P_{fuel}} \quad \eta_{th} = \frac{P_{th}}{P_{fuel}} \quad \eta_{tot} = \frac{P_{el} + P_{th}}{P_{fuel}} \quad (4)$$

2.2. Off-Design Modeling

The operating point of the single-shaft MGT derives from the interaction between the compressor and the turbine. Performance maps allow the off-design performance to be determined as a function of the inlet conditions and actual rotational speed (n) of the machine, by scaling from the design point conditions and speed. For the compressor and turbine,

respectively, the relationship between pressure ratio (β_c , β_{exp}) vs. corrected flow (CF, FF), with lines for each value of CS, was implemented by applying the following definitions:

$$CF = \frac{m_a \sqrt{\frac{T_{in,c}}{T_{ref}}}}{MW \frac{P_{in,c}}{P_{ref}}} \quad (5)$$

$$FF = \frac{C m_{exh}}{P_{in,t}} \sqrt{\frac{\left(\frac{R}{MW \gamma_{exh}}\right) T_{in,t}}{\left(\frac{2}{\gamma_{exh}+1}\right)^{\frac{\gamma_{exh}+1}{\gamma_{exh}-1}}}} \quad (6)$$

$$CS = n \sqrt{\frac{T_{ref}}{T_{in}}} \quad (7)$$

with $T_{ref} = 288.15$ K and $p_{ref} = 1.013$ bar. In Equation (6), the universal gas constant (R), molecular weight (MW) and specific heat ratio (γ) will be affected by changes in the exhaust composition because of fuel flexibility.

On each CS line, 10 points were defined with values of pressure ratio, corrected flow, and polytropic efficiency normalized with respect to design conditions, as follows:

$$\frac{CF}{(CF)_{Design Point}} \quad (8)$$

$$\frac{FF}{(FF)_{Design Point}} \quad (9)$$

$$\frac{CS}{(CS)_{Design Point}} \quad (10)$$

$$\frac{\beta}{(\beta)_{Design Point}} \quad (11)$$

$$\frac{\eta_y}{\eta_y - (\eta_y)_{Design Point}} \quad (12)$$

Moreover, for each CS line, the maximum pressure ratio, normalized by the nominal pressure ratio, is required to define surge for compressor and choking for the turbine. Eight speed lines were entered for each map.

3. Model Validation

This section is devoted to verifying the accuracy of the proposed model at both design and off-design conditions. Maps of the compressor and turbine were essential for evaluating the actual working point of each turbomachinery, by varying ambient temperature and load while maintaining the traditional fuel. As further demonstration of the method's reliability, syngas was also considered as a fuel source.

3.1. Nominal Conditions

In Table 3, Thermoflex model outputs (hereinafter referred to as "TFX") were compared against manufacturer's data at full load and ISO standard conditions: site elevation of 0 m above sea level; ambient temperature (T_{amb}) of 15 °C; relative humidity of 60%. The fuel type is NG. The design point is well simulated since the largest deviation between predicted and reference parameters is less than 2%. It should be noted that a tolerance of ± 3 kW and $\pm 1\%$ of the declared value was reported in [32] for electric power and efficiency, respectively. Moreover, it is worth highlighting that the slight overestimation of fuel LHV depends on NG composition: pure CH_4 was assumed in the model whereas a mixture of CH_4 (91% vol), C_2H_6 (7% vol), and C_3H_8 (2% vol) was considered in the datasheet [32]. It

was verified that this variation in the mixture of hydrocarbon gases entering the combustor, at the same fuel input, has a negligible impact on MGT performance: any difference in results is within the numerical error.

Table 3. Model validation at nominal conditions.

Parameter	Datasheet [32]	Model	Δ (%)
Fuel LHV (MJ/kg)	49.56	50.047	1.0
Fuel flow (kg/s)	0.00672	0.0068	1.2
Turbine inlet temperature (°C)	950	950	0
Turbine outlet temperature (°C)	650	652.9	0.4
Fuel input (kW)	333	338.1	1.5
Exhaust gas flow (kg/s)	0.8	0.8	0
Rotational speed (rpm)	70,000	70,000	0
Heat exchanger–inlet exhaust gas temperature (°C)	270	270	0
Heat exchanger–outlet exhaust gas temperature (°C)	70	70	0
Heat exchanger–inlet water temperature (°C)	50	50	0
Heat exchanger–outlet water temperature (°C)	70	70	0
Thermal power (kW)	165	165.7	0.4
Electric power (kW)	100	101.9	1.9
Electric efficiency (%)	30	30.14	0.5
Total efficiency (%)	80	79.1	−1.1

3.2. Effects of Ambient Temperature

The ambient temperature varied from -20 to 40 °C with 10 °C steps. Predictions were compared against the data available from [33]. Results are presented in Figure 2 as percent variation with respect to nominal condition ($T_{amb} = 15$ °C). Global parameters are shown together with the most significant MGT operating variables. As is well known, an increase in T_{amb} lowers the density of the air; thus, reducing m_a through the MGT with a negative effect on P_{el} . At the same time β_c is diminished whereas the compressor discharge temperature is increased; thus, impairing the prerequisites for the recuperator. Therefore, η_{el} is also decreased. Thermal power decreases much less than P_{el} because the reduction in m_{exh} is partially compensated by the augmentation of exhaust temperature at the recuperator inlet. This translates into an increasing temperature of the exhaust gas sent to the RHE, with a consequent benefit in terms of enhanced η_{th} . The behavior outlined above is valid at constant speed, which corresponds to $T_{amb} \geq 0$ °C. Obviously, the opposite takes place when lowering T_{amb} : an increase in η_{el} and P_{el} is expected. When the maximum capacity is reached at about 0 °C, power output is limited by gradually diminishing the rotational speed as T_{amb} falls below 0 °C, with a consequent declining trend in the intake air flow and, thus, β_c . This enables constant P_{el} , at about 120% of design value, while preserving η_{el} , which still shows increasing values with decreasing T_{amb} . Similarly, the profile of η_{th} does not appear to be influenced by speed reduction, despite the sharp fall in P_{th} at $T_{amb} < 0$ °C because of the drop in intake air.

Overall, the modeling procedure quite accurately reproduces the MGT performance discussed in [33]: P_{th} and air volume flow show similar trends; the same is valid for m_a and β_c , as pointed out by Caresana et al. All variables were properly calculated: the deviation between the actual value and the measured one is less than 4.5% for all global parameters such as P_{el} , η_{el} , P_{th} , and η_{th} . More precisely, the largest error is due to overestimation of P_{el} at of 40 °C. This might be due to the fact that computations were carried out with TIT held constant at the design value whereas a slight reduction in TIT, by up to 2% at the hottest T_{amb} , was considered in [33] to prevent the machine from thermal stresses.

Figure 3 depicts the impact of T_{amb} on rotating machineries. Two operating regimes are evident. Above the threshold of $T_{amb} = 0$ °C, at iso-speed conditions, the working points move towards lower β_c and lower CF as T_{amb} increases, along the equilibrium running line: in other words, the compressor delivers less air at a lower pressure hence MGT power decreases. On the turbine map, the corresponding reduction in β_{exp} can be appreciated;

values of FF are also diminished, although to a lesser extent than the compressor CF. Below the threshold of $T_{amb} = 0\text{ }^{\circ}\text{C}$, operating points deviate from the equilibrium running line: since the maximum capacity cannot be exceeded while lowering T_{amb} , rotational speed must be reduced. This means moving the working points towards lower corrected flows for the compressor whereas the opposite occurs for the turbine, as the decrease in $p_{in,t}$ outweighs the decrease in m_{exh} , at constant TIT (see Equation (6)).

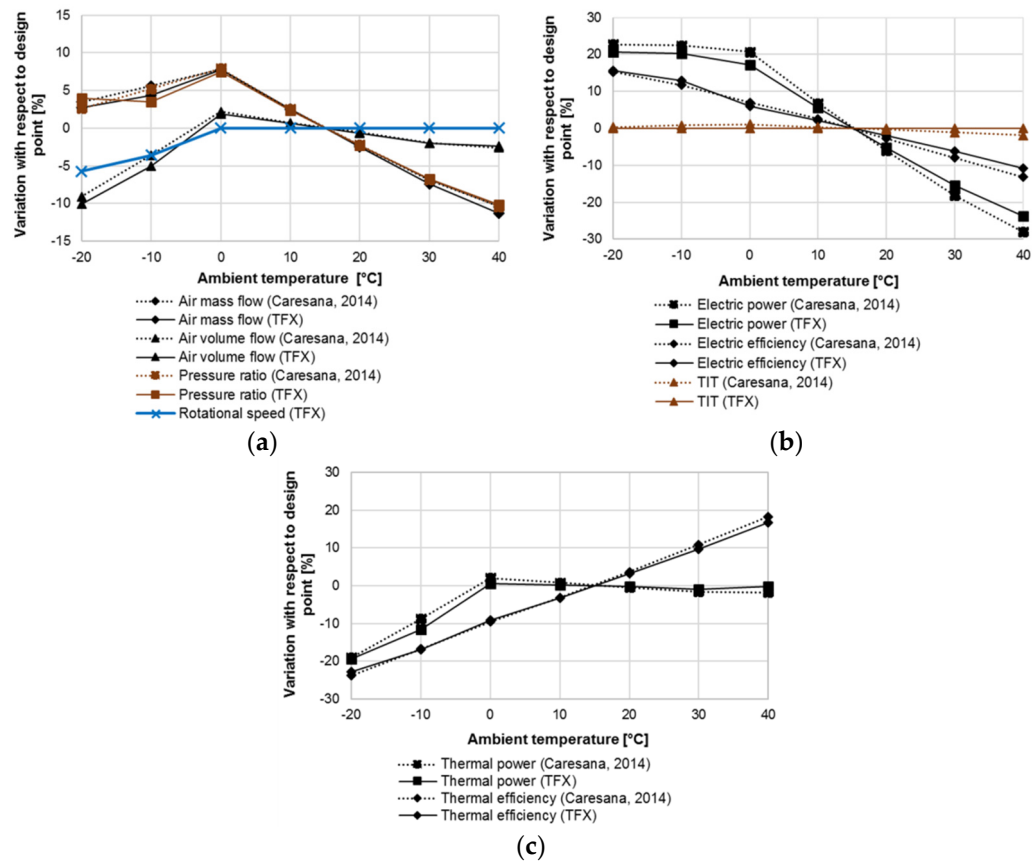


Figure 2. Model validation: effects of ambient temperature on (a) compressor characteristics; (b) electric power and efficiency; (c) thermal power and efficiency [33].

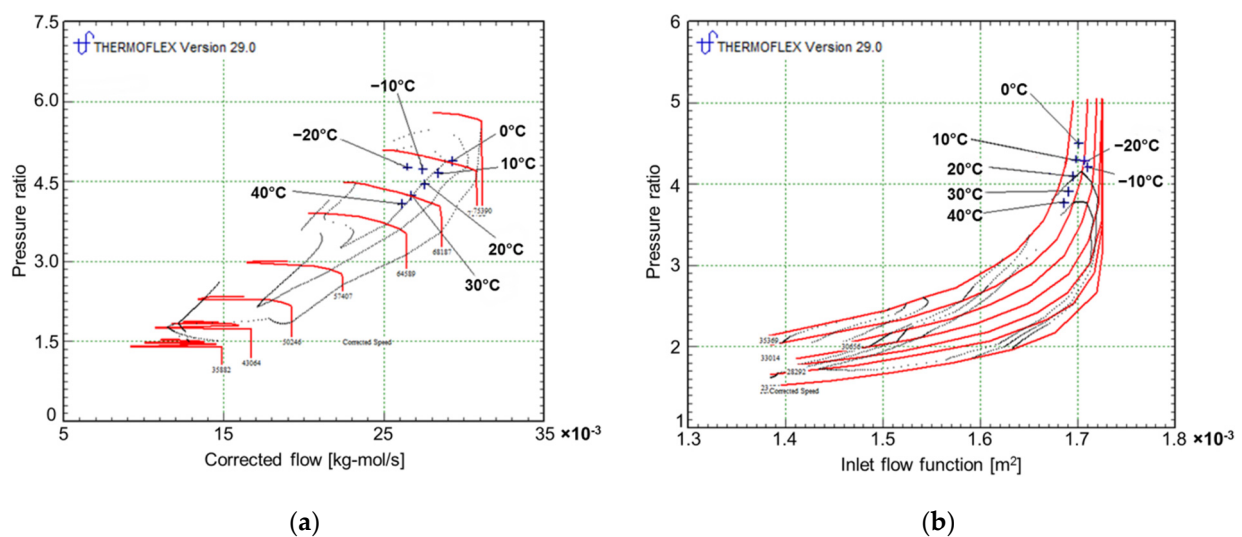


Figure 3. Effects of ambient temperature on performance maps of: (a) compressor; (b) turbine.

3.3. Effects of Part-Load Operation

Simulated cases reproduced the laboratory tests performed at T_{amb} of 8 and 30 °C, with ambient pressure of 101 kPa, under the same thermal load conditions. Measurements taken from [33] and model-predicted data are shown in Figure 4. The level of electric power was reduced up to 40 kW by lowering the rotational speed of the shaft. Looking at Figure 4a, η_{el} drops by about 4 pp, from 30% to 26%, when P_{el} falls from 100 to 40 kW. A loss in η_{el} of a similar magnitude occurs at $T_{amb} = 30$ °C when P_{el} is halved from 80 to 40 kW, although starting from a lower level. Conversely, higher values of P_{th} and η_{tot} can be achieved at hotter T_{amb} , when P_{el} stays below 80 kW.

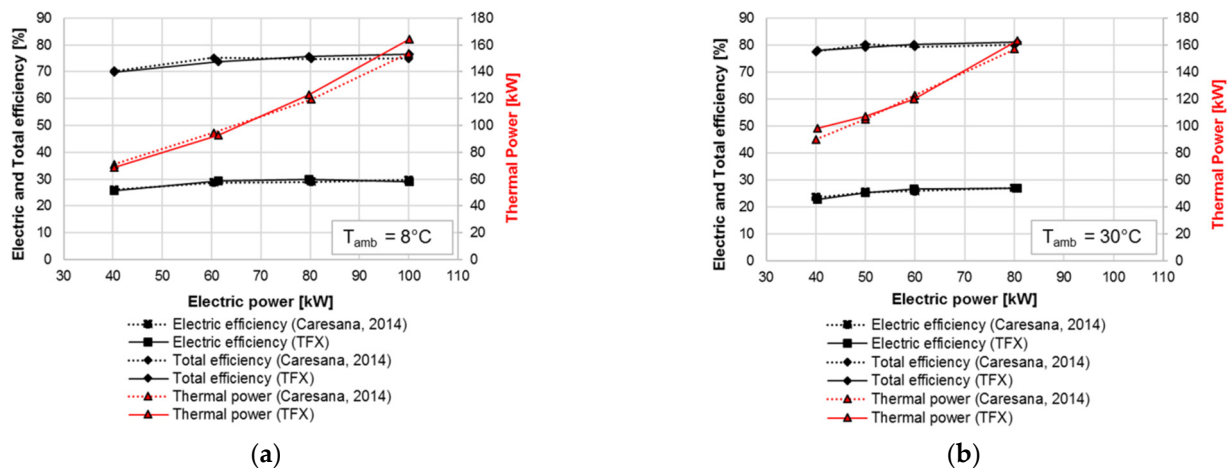


Figure 4. Model validation: effects of part-load operation at non-ISO conditions: (a) $T_{amb} = 8$ °C; (b) $T_{amb} = 30$ °C [33].

Good agreement between model-predicted and measured data is observed throughout the load range. Whatever T_{amb} , predictions of P_{th} at the ends of the considered range of P_{el} showed the largest deviations from measurements, still within 8%. A reason for this can be found in the management of the exhaust gas temperature at the recuperator outlet. Similar conclusions were obtained by Hampel and Braun [30]: they stated expressly that error in P_{th} mainly depends on overestimation of exhaust temperature at the recuperator outlet, since exhaust mass flow rate closely agrees with laboratory data across the entire load span. The investigation of part-load behavior at non-ISO conditions confirmed that lower air density, i.e., hotter T_{amb} , penalizes η_{el} but increases heat recovery at de-rated operation, once again consistently with [30].

3.4. Effects of Syngas Feeding

Drawing inspiration from the research carried out by Renzi et al. [35], syngas from pyrolysis of forestry residual biomass was chosen as fuel for validation purposes. Syngas composition is available, unlike the fuel conditions at the combustor inlet, which were set to avoid water condensation. Ultimate analysis prescribes the following (mol%): CH_4 (21%), H_2 (7%), CO_2 (38%), CO (29%), and H_2O (5%). Hence, LHV, being equal to 9.15 MJ/kg is less than a quarter of that of NG.

The model was used to check whether MGT can ensure in any case the nominal output at rated speed and ISO standard conditions. Please note that TIT was adjusted to 946 °C. Larger amount of syngas must be combusted, compared to NG, in order to release an equivalent amount of energy; thus, causing an increase in m_{exh} , hence in turbine power. The turbine adapts to new inlet conditions in terms of slightly reduced TIT and greater exhaust flow, with higher molecular weight (29.12 vs. 28.66). Indeed, variation in flue gas composition (mol%) takes place, unlike the previous cases: CO_2 increases from 1.5 to 4.2% at the expense of N_2 (74.3 vs. 76.1%), H_2O (3.5 vs. 4.0), and O_2 (17.1 vs. 17.4%). However, this only has a marginal influence on FF so that Figure 5b shows almost overlapping

turbine operating points for syngas and NG. Conversely, compressor operating point is deeply affected by fuel switching, as shown in Figure 5a: CF drops significantly whereas β_c increases slightly. Therefore, a reduced m_a exits the compressor at higher pressure, thereby causing the flow in the turbine, with larger β_t .

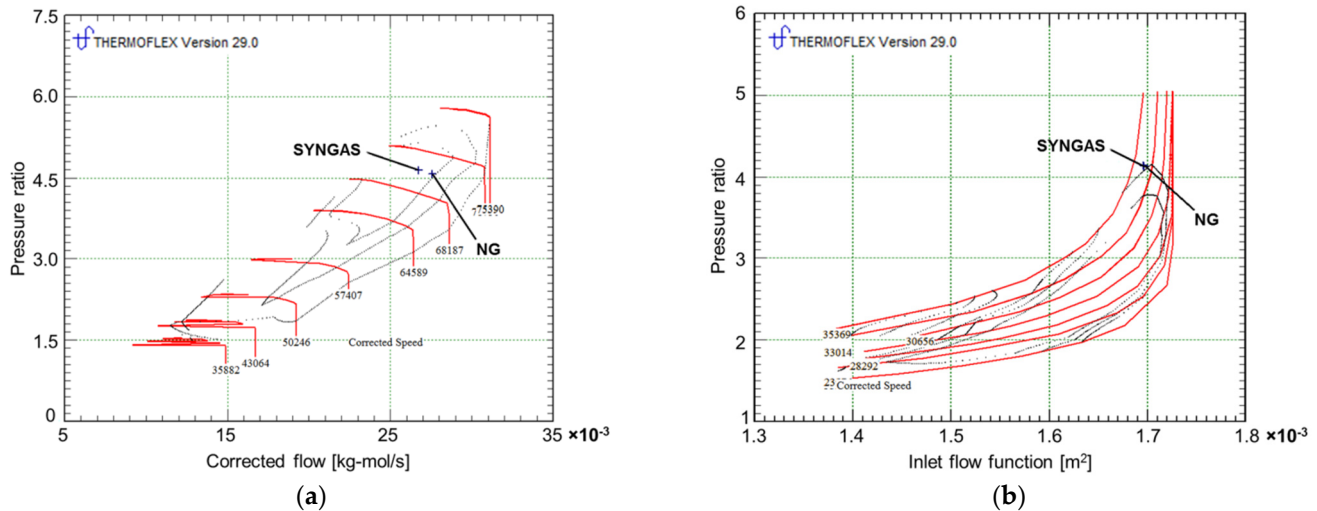


Figure 5. Effects of syngas feeding at rated speed on performance maps of: (a) compressor; (b) turbine.

Model outputs are collected in Table 4, for an easy comparison based on the results reported in [35]. With the largest percentage difference below 5%, the simulation captures well the effects of syngas feeding on MGT operation. Despite the slight underestimation of syngas flow and hence m_{exh} , which is responsible for underestimated turbine power by about 4%, turbomachineries are properly characterized in terms of η_{is} and β ; thus, supporting the correct application of performance maps. As regards η_{is} , the use of syngas in place of NG was found to enhance compressor performance (0.791 vs. 0.785) whereas the opposite is true for the turbine (0.812 vs. 0.829). This is fully in line with the findings presented in [35], just as the loss in η_{el} (29.26% vs. 30.14%) as the fuel input required to run the MGT at the rated speed is higher than that with NG (357 vs. 338 kW). Electricity production is also consistent with [35], being 2.4% higher than that with NG.

Table 4. Model validation with syngas feeding at the rated speed.

Parameter	Reference [35]	Model	Δ (%)
Syngas flow (kg/s)	0.0405	0.0386	−4.7
Air flow (kg/s)	0.77	0.7738	0.5
Exhaust flow (kg/s)	0.82	0.8123	−0.9
Compressor power (kW)	156.9	155.9	−0.6
Compressor outlet temperature (°C)	212.2	212.6	0.2
Pressure ratio (β_c)	4.55	4.62	1.5
Isentropic compressor efficiency ($\eta_{is,c}$)	0.788	0.791	0.4
Turbine power (kW)	294.7	281.6	−4.4
Expansion ratio (β_{exp})	4.14	4.26	2.9
Isentropic turbine efficiency ($\eta_{is,t}$)	0.827	0.812	−1.8

4. Results

As a complement to the majority of studies tackling combustion issues of NH_3/CH_4 mixtures, the effects of replacing NG with NH_3 on MGT performance were discussed by adjusting the power output to different loads, in view of achieving grid flexibility. The

picture was subsequently completed by a comparison between NG and NH_3 , used as pure fuel. Ammonia blending ratio (y_{NH_3}) varies between 0 and 1, according to the following:

$$y_{\text{NH}_3} = \frac{m_{\text{NH}_3}}{m_{\text{NH}_3} + m_{\text{CH}_4}} \quad (13)$$

Within the maximum combustor pressure of 7 bar, a preheater (labeled “Q+” in Figure 1) was included in the model to keep the temperature of gaseous ammonia at 50 °C; thus, avoiding liquefaction.

4.1. Full Load Behavior

A first set of simulations was carried out across the entire y_{NH_3} range while keeping rated specifications for TIT and P_{el} . Similarly to what was observed for the syngas feeding, a higher mass flow rate of NH_3 is required by the combustor, trying to compensate for the reduced LHV (18.6 MJ/kg), as compared with NG. The higher the y_{NH_3} , the larger the m_{fuel} (Figure 6a). The constraint of constant design power leads to a significant drop in the airflow entering the compressor (−4.5% at $y_{\text{NH}_3} = 1$), which ultimately leads to a reduction in m_{exh} as y_{NH_3} increases (−2.8% at $y_{\text{NH}_3} = 1$). Compressor CF is reduced as well, which translates into increasing β_c (Figure 6b). The same is valid for turbine β_{exp} which obviously stands at slightly lower level, because of pressure drops across the combustor and heat exchangers.

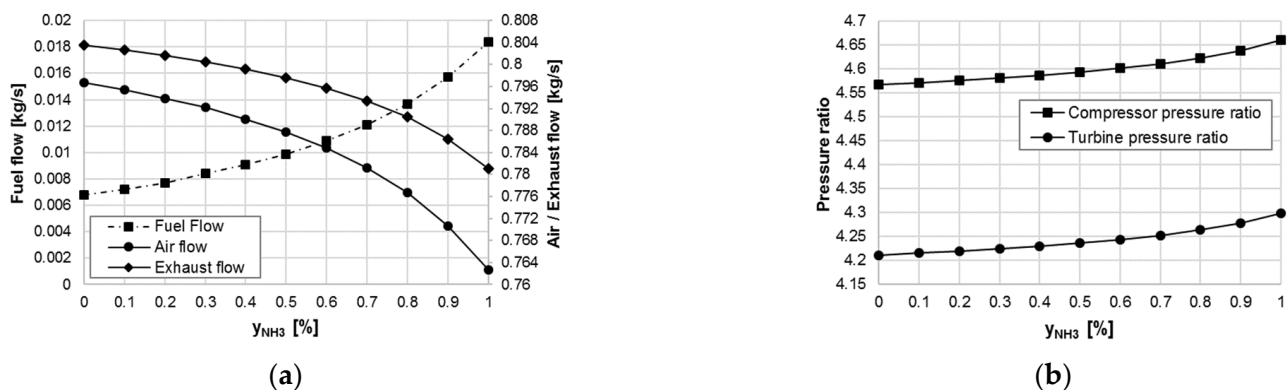


Figure 6. Effects of increasing ammonia blending ratio (y_{NH_3}) on: (a) mass flow rate of air, fuel, and flue gas; (b) compressor pressure ratio and turbine expansion ratio.

From Figure 7a it can be observed that the fuel input into the combustor increases with y_{NH_3} to guarantee the rated power output. This has a negative effect on η_{el} , whose value decreases by up to 0.5 pp at $y_{\text{NH}_3} = 1$ (from 29.5 to 29%). Conversely, heat recovery from exhaust gas is promoted as evident from the growing trend in P_{th} , with a consequent improvement in η_{th} , up to 0.5 pp (from 49.6% to 50.1%). It follows that the loss in η_{el} is compensated by the gain in η_{th} , as displayed in Figure 7b, so that η_{tot} remains almost constant, at about 79%, whatever y_{NH_3} . This result was corroborated by tests conducted on a 2 MW-class GT: η_{th} during NH_3 co-firing up 20% was found to stay constant at around 80%, at the same level as that during NG firing [36].

It should be clarified that the augmentation of P_{th} is due to the fact that the increase in exhaust temperature at the recuperator outlet (by up to 8 °C) outweighs the reduction in m_{exh} . On the other hand, despite the decrease in the heat transfer across the recuperator, reduced m_a may enter the combustor at increasing temperature. In addition, it was verified that turbine outlet temperature (TOT) exceeds the design value by 2 °C, at the worst.

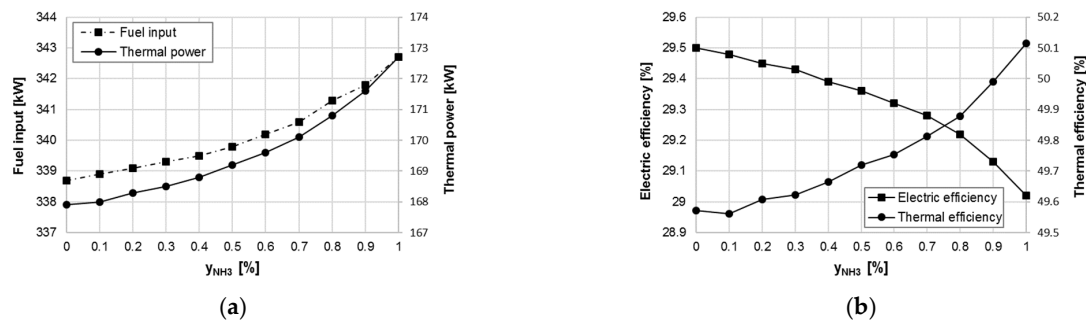


Figure 7. Effects of increasing ammonia blending ratio (y_{NH_3}) on: (a) fuel input and thermal power; (b) thermal end electric efficiency.

It deserves to be mentioned that, if the power constraint is removed, burning NH_3 would lead to an electric production by up to 113 kW, at $y_{NH_3} = 1$, still within the maximum capacity. Such a result could be achieved by running the MGT at the rated airflow: exhaust gas flow would increase up to 0.82 kg/s, still within the limit of 0.87 kg/s set by the manufacturer. Hence, P_{th} would increase as well, up to 176 kW. Therefore, conversion of MGT to pure NH_3 fuel operation could be accomplished. Indeed, power augmentation in the order of 10–20% has been known since 1968 when NH_3 replaced hydrocarbon in GT engines at the same TIT [37].

4.2. Part-Load Behavior

Three additional sets of simulations were executed at partial load by lowering P_{el} to 80, 60, and 40 kW, under the assumption of constant TIT, for consistency with Section 4.1. The findings obtained at full load remain valid from a qualitative point of view: trends shown in Figures 6 and 7 are confirmed. Whatever the MGT output, replacing NG with NH_3 causes the compressor working point to move towards lower CF and greater β_c (Figure 8a). The turbine is characterized by a slightly higher β_t and a small increase in FF, due to choked flow limit (Figure 8b). However, calculations at part-load gave the opportunity to discuss turbomachinery features while lowering the rotational speed. Operating points for both the compressor and turbine move downwards and left; thus, indicating a reduction in β and air/exhaust mass flow rate. Clearly, since less fuel input is required at part-load, the amount of NH_3 injected into the combustor gets smaller as P_{el} decreases: that is why the horizontal distance between extreme points (where y_{NH_3} equals 0 and 1, respectively) is shortened, with much more evident impact on compressor operation.

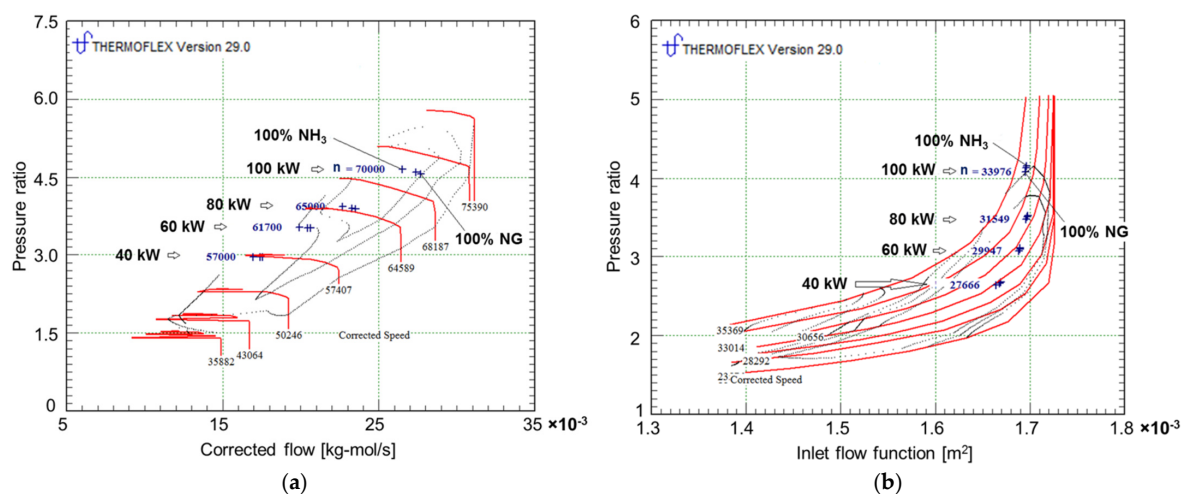


Figure 8. Effects of NH_3 feeding, at different levels of power output, on performance maps of: (a) compressor; (b) turbine.

The compressor seems to be severely affected by partial load (Figure 9a): $\eta_{is,c}$, which was found to be enhanced by raising y_{NH_3} at full load, goes completely the other way when P_{el} equals 80 and 60 kW. The largest loss in $\eta_{is,c}$ is within 0.3 and 0.6 pp, respectively. However, $\eta_{is,c}$ stays above 78.8% if P_{el} does not fall below 60 kW, even though the compressor approaches its surge limit. The case at $P_{el} = 40$ kW is associated with the lowest value of $\eta_{is,c}$ which is stable at 75.5%; thus, underlining that MGT performance may degrade significantly at low load conditions. On the contrary, the turbine behaves in the same manner, whatever the P_{el} level (Figure 9b): $\eta_{is,t}$, despite the declining trend as y_{NH_3} increases, remains at good level amounting to at least 80%. Nevertheless, fuel switching has an adverse influence on turbine performance.

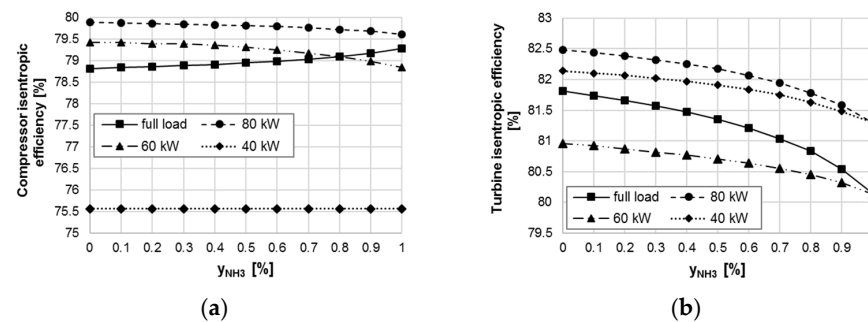


Figure 9. Effects of NH_3 feeding, at different levels of power output, on isentropic efficiency of: (a) compressor; (b) turbine.

As far as the energy balance is concerned, nothing changes with respect to the results in Figure 7b. In fact, the efficiency penalty is confirmed when referring to η_{el} : the largest loss, at $y_{NH_3} = 1$, lies between 0.4 and 0.6 pp in comparison with NG feeding (Figure 10a). On the contrary, η_{th} rises to the same extent, whatever the load (Figure 10b). It turned out that η_{tot} is not influenced by y_{NH_3} : trends substantially flat are depicted in Figure 10c, at gradually decreasing levels, i.e., 78.4, 77.1, 74.2%, while lowering the power in steps of 20 kW.

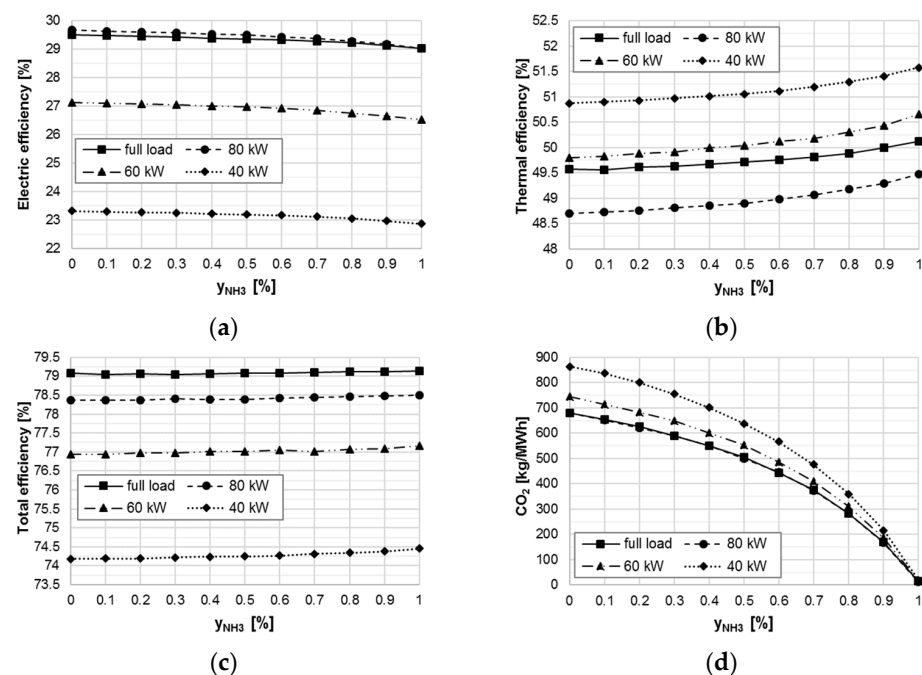


Figure 10. Effects of NH_3 feeding, at different levels of power output, on: (a) electric efficiency; (b) thermal efficiency; (c) total efficiency; (d) CO_2 emission intensity.

However, the main goal is to reduce greenhouse gas emissions. CO₂ emission intensity decreases continuously with the effect of using NH₃ instead of NG, whatever P_{el} (Figure 10d). It is important that the amount of CO₂ discharged through the stack can be brought down to zero not only at full load, the condition at which the largest emission equals 680 kg/MWh, but especially at part-load, which is characterized by higher emission intensity, up to 864 kg/MWh. In terms of flue gas composition, CO₂ is simply being replaced by H₂O, as a product of NH₃ combustion. In fact, the content of N₂ and O₂ undergoes a small reduction, by a maximum of 3%.

4.3. Natural Gas vs. Ammonia

One might argue that keeping TIT constant at part-load would inevitably set demands for the recuperator materials. Indeed, TOT was found to raise from 650 °C, at full load, up to 733 °C, at 40% load. Moreover, firing of 100% ammonia led to a negligible increase in TOT, by 2 °C, compared to pure NG. The point is that the MGT electric output may be reduced by lowering both rotational speed and TIT, to prevent temperature increase in the combustion gases at the recuperator inlet [38]. Accordingly, simulations at part-load were repeated using the same levels of rotational speed as Section 4.2, but with decreasing TIT as P_{el} reduces. TIT values, being determined in such a way that TOT exceeds the design value by 10 °C at the worst, are equal to 920, 895, and 870 °C at 80, 60, and 40 kW of power, respectively. Results shown in Figure 11 allow a direct comparison between NG and NH₃, used as pure fuel. At first glance, the part-load strategy has a marginal effect on MGT performance, thereby confirming the results presented in Section 4.2: although NH₃ may lower η_{el} by 0.5 pp, η_{tot} is not less than that with NG thanks to enhanced heat recovery. However, at $P_{el} < 60$ kW, there is a slightly more marked drop in η_{el} when TIT is lowered with load, whatever the fuel. Since a decrease in η_{el} contributes to the heat output, but in practice P_{th} falls at part-load because of reduced m_{exh} , the decay in η_{tot} at de-rated conditions is roughly the same, regardless of fuel type and part-load control.

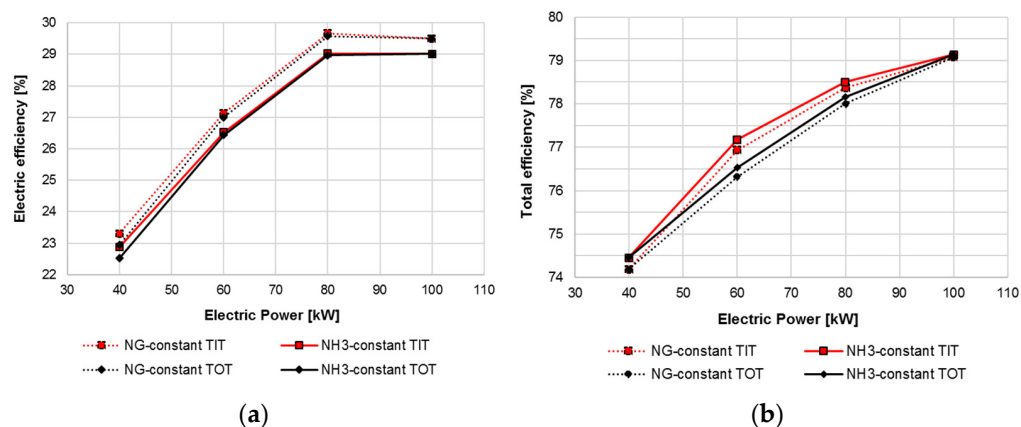


Figure 11. Effects of replacing NG with NH₃, by varying part-load control strategy, on: (a) electric efficiency; (b) thermal efficiency.

5. Conclusions

Within the context of distributed generation, MGT is an attractive prime mover fed by a relatively clean fossil fuel such as NG. However, in fulfilling the goal of carbon neutrality, carbon-free fuels such as ammonia have gained increased interest as they can be used as energy carriers in a circular carbon economy.

In this study, a modeling procedure was developed, tested, and used to predict the performance of a MGT flexible in operation, in terms of load reduction and fuel switching. Model predictions of electric and thermal efficiency at non-ISO conditions and part-load were validated against data sources, using NG as fuel. Further verification, to ensure that the model replicates experiments satisfactorily, included adoption of syngas as the fuel, at a rated speed. Steady-state simulations were then run for evaluating the impact of ammonia

combustion on MGT thermodynamic behavior. Substantial changes, with respect to the conventional fuel, can be summarized as follows:

- At the same MGT power output, compressor–turbine matching in a single-shaft arrangement results in lower flow rates of air and flue gas, despite the increase in the fuel amount due to reduced LHV.
- The compressor operating point moves towards lower CF and slightly higher β_c ; the turbine is affected by a small increase in β_t and FF. Isentropic efficiency varies within 1.6 pp.
- Although η_{el} is lowered by about 0.5 pp, η_{tot} shall remain unaffected thanks to enhanced heat recovery. This applies to the entire load range, from 100 to 40%, whatever the part-load strategy (i.e., keeping TIT/TOT constant).
- CO₂ content in flue gas may be reduced down to zero, offset by H₂O.

In conclusion, there are no disadvantages of burning ammonia in a MGT for CHP applications, although adjustment of the turbomachinery operating point is required. However, NO_x emissions are relatively high in practical combustion; therefore, selective catalytic reduction systems may be installed to reduce stack NO_x concentration. Finally, the scale of facilities in experimental research fits well with MGT; thus, enabling advancements in burner technology.

Author Contributions: Conceptualization, S.R.; methodology and software, V.B. and S.R.; validation and simulation, V.B.; writing—original draft preparation, S.R. and V.B.; writing—review and editing, S.R.; supervision, S.R. All authors have read and agreed to the published version of the manuscript.

Funding: This research received no external funding.

Institutional Review Board Statement: Not applicable.

Informed Consent Statement: Not applicable.

Data Availability Statement: Not applicable.

Conflicts of Interest: The authors declare no conflict of interest.

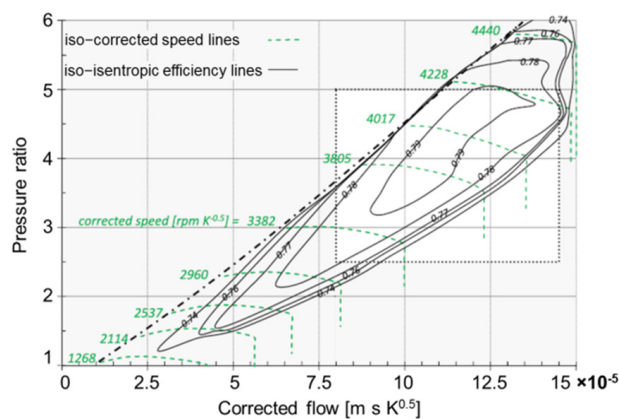
Abbreviations

C	Dimensional constant
CF	Compressor corrected flow
CHP	Combined heat and power
CS	Corrected speed
DME	Dimethyl ether
FF	Turbine inlet flow function
GT	Gas turbine
LHV	Lower heating value
m	Mass flow rate
MGT	Micro gas turbine
MW	Molecular weight
n	Rotational speed
NG	Natural gas
P	Power
p	Pressure
pp	Percentage points
R	Gas constant
RHE	Recovery heat exchanger
T	Temperature
TFX	Thermoflex predictions
TIT	Turbine inlet temperature
TOT	Turbine outlet temperature

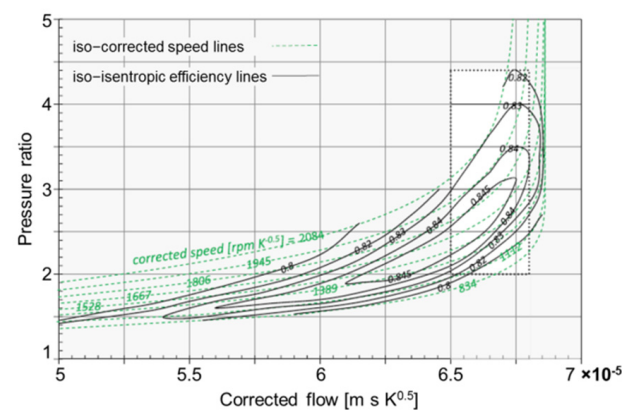
y	Ammonia blending ratio
β	Pressure ratio
γ	Ratio of specific heat
η	Efficiency

Subscripts

a	air
amb	ambient
c	compressor
el	electric
exh	exhaust
exp	expansion
fuel	fuel input
in	inlet
is	isentropic
out	outlet
ref	reference
t	turbine
tot	total
y	polytropic

Appendix A

(a)



10. Wan, Z.; Tao, Y.; Shao, J.; Zhang, Y.; You, H. Ammonia as an effective hydrogen carrier and a clean fuel for solid oxide fuel cells. *Energy Convers. Manag.* **2021**, *228*, 113729. [CrossRef]
11. Kobayashi, H.; Hayakawa, A.; Somarathne, K.K.A.; Okafor, E.C. Science and technology of ammonia combustion. *Proc. Combust. Inst.* **2019**, *37*, 109–133. [CrossRef]
12. Valera-Medina, A.; Xiao, H.; Owen-Jones, M.; David, W.I.; Bowen, P.J. Ammonia for power. *Prog. Energy Combust. Sci.* **2018**, *69*, 63–102. [CrossRef]
13. Xu, X.; Liu, E.; Zhu, N.; Liu, F.; Qian, F. Review of the Current Status of Ammonia-Blended Hydrogen Fuel Engine Development. *Energies* **2022**, *15*, 1023. [CrossRef]
14. Karabeyoglu, A.; Evans, B. Selection of NH₃ for Gas Turbine Use. In Proceedings of the 8th NH₃ Conference, Portland, OR, USA, 19 September 2011.
15. Kurata, O.; Iki, N.; Matsunuma, T.; Inoue, T.; Tsujimura, T.; Furutani, H.; Kobayashi, H.; Hayakawa, A. Performances and emission characteristics of NH₃-air and NH₃CH₄-air combustion gas-turbine power generations. *Proc. Combust. Inst.* **2017**, *36*, 3351–3359. [CrossRef]
16. Kurata, O.; Iki, N.; Matsunuma, T.; Inoue, T.; Tsujimura, T.; Furutani, H.; Hayakawa, A.; Kobayashi, H. Success of Ammonia-fired, Regenerator-Heated, Diffusion Combustion Gas Turbine Power Generation and Prospect of Low NO_x Combustion with High Combustion Efficiency. In Proceedings of the ASME 2017 Power Conference Joint with ICOPE-17, Charlotte, NC, USA, 26–30 June 2017.
17. Iki, N.; Kurata, O.; Matsunuma, T.; Inoue, T.; Tsujimura, T.; Furutani, H.; Kobayashi, H.; Hayakawa, A. Operation and Flame Observation of Micro Gas Turbine Firing Ammonia. In Proceedings of the ASME Turbo Expo 2017: Turbomachinery Technical Conference and Exposition, Charlotte, NC, USA, 26–30 June 2017.
18. Pugh, D.; Bowen, P.; Valera-Medina, A.; Giles, A.; Runyon, J.; Marsh, R. Influence of steam addition and elevated ambient conditions on NO_x reduction in a staged premixed swirling NH₃/H₂ flame. *Proc. Combust. Inst.* **2019**, *37*, 5401–5409. [CrossRef]
19. Pugh, D.; Valera-Medina, A.; Bowen, P.; Giles, A.; Goktepe, B.; Runyon, R.; Morris, S.; Hewlett, S.; Marsh, R. Emissions performance of staged premixed and diffusion combustor concepts for an NH₃/air flame with and without reactant humidification. *J. Eng. Gas Turbines Power* **2021**, *143*, 051012. [CrossRef]
20. Božo, M.G.; Viguera-Zuniga, M.O.; Buffi, M.; Seljak, T.; Valera-Medina, A. Fuel rich ammonia-hydrogen injection for humidified gas turbines. *Appl. Energy* **2019**, *251*, 113334. [CrossRef]
21. Ditaranto, M.; Saanum, I.; Larfeldt, J. Experimental Study on High Pressure Combustion of Decomposed Ammonia: How Can Ammonia Be Best Used in a Gas Turbine? In Proceedings of the ASME Turbo Expo 2021: Turbomachinery Technical Conference and Exposition, Virtual, 7–11 June 2021.
22. Han, X.; Wang, Z.; Costa, M.; Sun, Z.; He, Y.; Cen, K. Experimental and kinetic modeling study of laminar burning velocities of NH₃/air, NH₃/H₂/air, NH₃/CO/air and NH₃/CH₄/air premixed flames. *Combust. Flame* **2019**, *206*, 214–226. [CrossRef]
23. Okafor, E.C.; Naito, Y.; Colson, S.; Ichikawa, A.; Kudo, T.; Hayakawa, A.; Kobayashi, H. Experimental and numerical study of the laminar burning velocity of CH₄-NH₃-air premixed flames. *Combust. Flame* **2018**, *187*, 185–198. [CrossRef]
24. Wang, S.; Wang, Z.; Elbaz, A.M.; Han, X.; He, Y.; Costa, M.; Konnov, A.A.; Roberts, W.L. Experimental study and kinetic analysis of the laminar burning velocity of NH₃/syngas/air, NH₃/CO/air and NH₃/H₂/air premixed flames at elevated pressures. *Combust. Flame* **2020**, *221*, 270–287. [CrossRef]
25. Yin, G.; Li, J.; Zhou, M.; Li, J.; Wang, C.; Hu, E.; Huang, Z. Experimental and kinetic study on laminar flame speeds of ammonia/dimethyl ether/air under high temperature and elevated pressure. *Combust. Flame* **2022**, *238*, 111915. [CrossRef]
26. Chiong, M.C.; Chong, C.T.; Ng, J.H.; Mashruk, S.; Chong, W.W.F.; Samiran, N.A.; Mong, G.R.; Valera-Medina, A. Advancements of combustion technologies in the ammonia-fuelled engines. *Energy Convers. Manag.* **2021**, *244*, 114460. [CrossRef]
27. Keller, M.; Koshi, M.; Otomo, J.; Iwasaki, H.; Mitsumori, T.; Yamada, K. Thermodynamic evaluation of an ammonia-fueled combined-cycle gas turbine process operated under fuel-rich conditions. *Energy* **2020**, *194*, 116894. [CrossRef]
28. Božo, M.G.; Valera-Medina, A. Prediction of novel humidified gas turbine cycle parameters for ammonia/hydrogen fuels. *Energies* **2020**, *13*, 5749. [CrossRef]
29. Ayaz, S.K.; Altuntas, O.; Caliskan, H. Effect of ammonia fuel fraction on the exergetic performance of a gas turbine. *Energy Procedia* **2018**, *144*, 150–156. [CrossRef]
30. Hampel, C.A.; Braun, R.J. Off-design modeling of a microturbine combined heat & power system. *Appl. Therm. Eng.* **2022**, *202*, 117670.
31. Reale, F.; Sannino, R. Numerical Modeling of Energy Systems Based on Micro Gas Turbine: A Review. *Energies* **2022**, *15*, 900. [CrossRef]
32. Technical description-T100 NG. D 14127-03 Version 3 09/12/29, Copyright © 2009 Turbec Spa. Available online: www.turbec.com (accessed on 5 January 2010).
33. Caresana, F.; Pelagalli, L.; Comodi, G.; Renzi, M. Microturbogas cogeneration systems for distributed generation: Effects of ambient temperature on global performance and components' behavior. *Appl. Energy* **2014**, *124*, 17–27. [CrossRef]
34. Deployment of FlexCHP System. Available online: <https://www.osti.gov/servlets/purl/1238362> (accessed on 20 April 2022).
35. Renzi, M.; Patuzzi, F.; Baratieri, M. Syngas feed of micro gas turbines with steam injection: Effects on performance, combustion and pollutants formation. *Appl. Energy* **2017**, *206*, 697–707. [CrossRef]
36. Ito, S.; Uchida, M.; Suda, T.; Fujimori, T. Development of ammonia gas turbine co-generation technology. *IHI Eng. Rev.* **2020**, *53*, 1–6.

-
37. Bull, M.G. *Development of an Ammonia-Burning Gas Turbine Engine*; Solar Turbines International: San Diego, CA, USA, 1968.
 38. Backman, J.L.H.; Kaikko, J. Microturbine Systems for Small Combined Heat and Power (CHP) Applications. In *Small and Micro Combined Heat and Power (CHP) Systems*; Woodhead Publishing: Sawston, UK, 2011; pp. 147–178.